

Kinetic energy functionals, the N -representability of the pair-density, and illustrative calculations via the classical map hyper-netted-chain (CHNC) method.

M.W.C. Dharma-wardana

National Research Council of Canada, Ottawa, Canada, K1A 0R6 *

(Dated: July 30, 2019)

The classical-map hyper-netted-chain (CHNC) method in the theory of interacting electrons uses a kinetic energy functional in the form of a classical-fluid temperature. Here we show that the CHNC pair distribution functions (PDFs) correspond to N -representable densities. Since the PDFs of a system are sufficient to obtain the equation of state as well as linear-response properties of electron-ion systems, we review the CHNC method for completely classical calculations of electron-ion systems in the quantum regime, using hydrogen as an example since quantum Monte Carlo (QMC) comparisons are available. We also present neutral pseudo-atom (NPA) calculations which use rigorous density-functional theory (DFT) based single-center reductions of the N -ion simulation problem. The PDFs of a 2D electron-hole system are given as an example of 2D-warm dense matter where the electrons and the counter particles are all in the quantum regime. The CHNC PDFs and NPA results agree well with the ion-ion, electron-ion and electron-electron PDFs (where available) obtained via computationally limiting methods like QMC, or DFT coupled to molecular dynamics simulations. The CHNC methods scale as the zeroth power of the number of particles treated.

PACS numbers: 31.10.+z, 71.10.-w, 71.15.Nc, 72.20.Ht

INTRODUCTION

The wavefunction $\Psi(\vec{r}_1, \dots, \vec{r}_N, \{\vec{R}_j\})$ of an N -electron quantum system depends on $3N$ space coordinates, spin indices, as well as coordinates $\{\vec{R}_j\}$ specifying the configuration of the nuclei present in the system. In the following at first the ions are treated as passively providing an ‘external potential’ to the electrons. In the final section the two component system of interacting electrons and ions are treated.

In most cases the ions behave ‘classically’, while the electrons are quantum mechanical. We seek to represent the electrons even at the extreme quantum limit of $T = 0$ by an ‘equivalent’ classical Coulomb fluid (CCF), at least in a statistical sense. For instance, the CCF should have the same pair distribution functions (PDFs) as the electron system. Such maps need to satisfy the N -representability constraints that apply to all quantum densities [1, 2].

The many-electron wavefunction contains significantly more information than necessary for calculating measurable properties of physical systems. As N becomes large, the resolutions of the many-particle Schrodinger or Dirac equation, or their quantum Monte Carlo (QMC) implementations become numerically prohibitive. A way out is presented by the Hohenberg-Kohn theorem basic to density functional theory (DFT), which asserts that the ground-state energy E of the N -particle system is a functional of just the *one-body* electron density $n(r)$ [3–5].

$$n(r) = \int d\vec{r}_2 \dots d\vec{r}_N |\Psi(\vec{r}_1, \dots, \vec{r}_N)|^2, \quad (1)$$

The Hohenberg-Kohn theorem is a counter-intuitive re-

sult since the many-particle Hamiltonian

$$H = T + V(\vec{r}) + V_{ee}(\vec{r}_1, \vec{r}_2) \quad (2)$$

explicitly contains the electron-electron Coulomb potential – a two-body interaction. The many-body effects of this interaction, as well as corrections arising from the kinetic energy operator T acting on the many-body wavefunction Ψ are contained in a one-body energy functional known as the XC-functional of DFT, viz, $E_{xc}([n])$. Since the exchange energy component E_x of the Hartree-Fock energy is explicitly known, the correlation energy E_c can be independently considered. However, the grouping of E_x and E_c together is justified (especially for free-electron systems like metals and plasmas at finite- T) due to important cancellations between the two terms [6].

$$H\Psi = E\Psi, \quad E = E_{\text{HF}} + E_c. \quad (3)$$

Here E_{HF} is the ‘mean-field’ or Hartree-Fock energy of the electron system. The relevant many-body corrections are in the XC-functional whose functional derivative with respect to the one-body density gives the Kohn-Sham one-body XC-potential. Whether such a potential exists leads to the V -representability problem briefly discusses near the conclusion.

The Hohenberg-Kohn theory posits that the exact ground state one-body density $n(r)$ is precisely the one which minimizes the ground state energy. Its extension to finite- T [7] states that the Helmholtz free energy F of the system is a functional of the one-body density, and that F is a minimum for the true density. The finite- T theory is considered to be more robust than the $T = 0$ theory, e.g., when magnetic fields are included [8, 9].

It was already recognized prior to DFT that the ground state energy can be expressed entirely in terms of the two-body density $n(\vec{r}_1, \vec{r}_2)$, but a reduction to a one-body

functional was not suspected. The two-body density matrix is obtained by integrating all but two of the space and spin variables of the N -body density, i.e., $|\Psi(\vec{r}_i)|^2$. This is also known as the two-particle reduced density matrix (2-RDM), and identifies with the PDF itself (depending on the prefactors used). The pair-distribution function $g(\vec{r}_1, \vec{r}_2)$ reduces to $g(r)$ for a uniform system, and gives the probability of finding a second particle at the radial distance r , with the first particle at the origin.

The one-body density in a system where the origin of coordinates is attached to one of the particles automatically becomes a 2-body density in the laboratory frame, and hence the PDF of homogeneous systems, e.g., a uniform Coulomb fluid, can be used to display the inherent particle correlations in a uniform fluid.

$$n(\vec{r}_1=0, \vec{r}_2=\vec{r}) = \bar{n} g_{12}(r).$$

While placing the origin on a classical particle is possible, more care is needed in the quantum problem of the uniform electron liquid (UEL) to be discussed below.

In 1955 Mayer proposed [10] to compute the ground-state energy of N -electron systems variationally as a functional of the two-electron RDM, i.e., the PDF, instead of the many-body wavefunction. Both Ψ , and the 2-RDM are unknown, but, unlike the wavefunction, the 2-RDM has the advantage that its application scales polynomially with the number N of electrons. However, the 2-electron RDM must be a reduction of an N -body wavefunction for it to be a physically acceptable 2-density. Otherwise, the ground state energy for $N > 2$ can even fall below the true ground state energy during a variational calculation. So the 2-electron RDM must be constrained to represent an N -electron wavefunction. Coleman called these constraints N -representability conditions [1]. The Hohenberg-Kohn minimization must be constrained to satisfy the requirements of N -representability [11, 12].

The implementation of DFT used in the original Kohn-Sham theory [4] maps the interacting electrons to a set of non-interacting electrons at the *interacting density*, and calculates the ‘Kohn-Sham’ one-electron wavefunctions $\phi_j(r)$ using a local-density approximation (LDA) to the exchange-correlation potential. Hence the corresponding many-body wavefunction is a single Slater determinant, and the Kohn-Sham theory gives rise to the N -representable density $n(r)$ given by:

$$n(r) = \sum_j |\phi_j(r)|^2 f(\epsilon_j). \quad (4)$$

At $T = 0$ the Fermi occupation factors $f(\epsilon_j)$ reduce to unity or zero for occupied and unoccupied states. Hence the summation at $T = 0$ is over occupied states, while at finite- T such summations, and the required basis sets become rapidly prohibitive as T increases. The KS $\phi_j(r)$, ϵ_j have the physical meaning of being the eigenstates and

eigenenergies of the fictitious non-interacting electron map of the interacting electron system, rather than those of the original interacting electron system. The Kohn-Sham procedure guarantees the N -representability of the density by treating the kinetic energy operator explicitly, without using a kinetic energy (K.E.) functional as in Hohenberg-Kohn DFT.

The simplest K.E. functional is that used in Thomas-Fermi theory. Various extensions of Thomas-Fermi theory under the name of ‘orbital-free’ DFT, as well as practical applications continue to be relevant [5, 13–17]. Many formulations use the Weiszacker ansatz where just one orbital, viz., $\phi(r) = \sqrt{n(r)}$ is used in a Schrödinger-like equation to obtain the kinetic energy. However, the non-local nature of the kinetic energy operator continues to be a great stumbling block. The excellent review by Carter [13], littered with many acronyms, shows the highly heuristic nature of the search for a K.E. functional that has continued for some four score years.

A K.E. functional is unnecessary for simple ‘one-center’ calculations which are very rapid, and typical in atomic physics or with the neutral-pseudo-atom (NPA) model, originally proposed for solids [18], and adapted to finite- T metallic fluids and plasmas [19–23]. The NPA has been formulated in a number of different ways [24–27]. Here we follow the model of Ref. [21] which is a simplification of [19] and adapted to multi-component finite- T calculations. In these NPA models of electron-ion systems, the many-ion problem is replaced by a ‘one-ion’ problem, while the many-electron problem is replaced by a single-electron KS problem. However, in simulations done with codes like the VASP [28] or ABINIT [29] the many-ion problem is *not* reduced. Instead, they explicitly use some 100-200 nuclear centers, say N_I , and even up to $N = N_e \sim 1000$ electrons in thousands of steps of KS and molecular-dynamics (MD) calculations. Hence such methods are extremely expensive and become prohibitive for many problems in warm-dense matter, materials science and biophysics. However, they provide useful benchmarks in simplified limits.

Such N_I -ion quantum calculations can be greatly simplified as follows.

1. By the construction of an explicit electron kinetic energy functional in terms of the one-body electron density $n(\vec{r})$.
2. Using a neutral pseudo-atom approach where the N_I nuclei are replaced by a one-body ion distribution $\rho(\vec{r})$ [19, 20], while the electrons are described as usual by the distribution $n(\vec{r})$ from KS theory as described below. Since ions are classical particles, in most applications, an ion is chosen as the origin of coordinates with no loss of generality. Two coupled KS-equations for the two subsystems (ions and electrons) arise from the functional differentiation of the free energy.

$$\frac{\delta F([n], [\rho])}{\delta [n]} = \mu_e, \quad \frac{\delta F([n], [\rho])}{\delta [\rho]} = \mu_I. \quad (5)$$

The electron and ion chemical potentials appear on the RHS. The first equation reduces to a one-center Kohn-Sham equation for the electrons in the field of the ion at the origin, while the second equation defines a classical distribution around the origin containing an ion-correlation functional, and reduces to an HNC-like equation [19, 20]. If there are many types of ions, a coupled set of one-center equations appear [21].

This approach to interacting electron-ion systems does not invoke the Born-Oppenheimer (BO) approximation, but the use of BO can further simplify the implementation. The solution of such one-center equations is numerically extremely rapid, even at finite T . Such calculations reproduce the PDFs $g_{cc}(r)$ of, say, molten carbon (or silicon) containing a complex bonding structure that are only exposed by taking ‘snap shots’ in lengthy and expensive DFT-MD simulations. That is, the *one-center* NPA calculations include sufficiently good ion-ion classical correlation functionals such that they are able, e.g., to reproduce the peak in the $g_{cc}(r)$ that correspond to the 1.4-1.5Å C-C covalent bond as well the peaks in the $g(r)$ due to the hard sphere-like packing effects seen in DFT-MD simulations [22, 23].

3. The NPA approach can also be further simplified by the use of a K.E. functional; but the NPA calculation is already so rapid that nothing is gained on using approximations to the K.E. functional that bring in their own errors.

Several models use the the name “Neutral Pseudo Atom”, but there are significant differences. Thus Chihara uses a neutral-pseudo-atom construction where he begins from the HNC equation and identifies a ‘quantum’ Ornstein-Zernike equation applicable to electrons as well [27]. While this is reasonable for ion-ion correlations, and perhaps even for electron-ion correlations, its validity for quantum electrons is debatable. Thus Anta and Louis [25] in their implementation of an NPA using Chihara’s ‘quantal HNC (qHNC)’ scheme cautiously avoid the use an e-e qHNC equation. The NPA approach proposed by the present author and Perrot simply uses DFT for both electrons and ions, and invokes the HNC diagrams, bridge diagrams and the Ornstein-Zernike (OZ) equation only to construct an ion-ion correlation functional [19, 21].

In contrast, in the CHNC the electrons are replaced by a *classical* Coulomb fluid having the same PDFs as quantum electrons. Hence we only need to use the classical

OZ and HNC equations regarding which there should be no controversy. However, unlike the NPA, it does not explicitly use a KS-equation. Hence the N -representability of the pair-densities obtained from the method needs to be addressed.

Several exact requirements on the K.E. functional (such as positivity) and their violation in various implementations has been noted [30, 31]. On the other hand, whether ‘orbital-free’ formulations lead to N -representable densities, or non-negative electron-electron pair-distribution functions etc., do not seem to have been studied. Even without such tests, that calculations using K. E. functionals are far less accurate than KS calculations is well known. Furthermore, energies from such calculations may fall *below* the exact energies, as the approximate K.E. functionals may not satisfy N -representability constraints. In fact, even some Kohn-Sham calculations that use generalized gradient approximations show such anomalies [32].

The study of the electron distribution in a uniform electron liquid (UEL) when a ‘test electron’ is placed at the origin naturally leads to the question of the direct calculation of the physically valid $g_{ee}(r)$ of the UEL rather than for a ‘test particle’. Here the electron kinetic energy functional must satisfy the required constraints, and also avoid any *selection* of an ‘electron’ held at the origin whereby it is made into a specific ‘test particle’. A way around such problems is possible if a valid ‘classical representation’ of the quantum electrons were available, at least in a statistical sense [33].

We recapitulate the classical-map hyper-netted-chain (CHNC) scheme for the convenience of the reader. It has been used successfully [33–36] for a number of uniform systems, namely, 3D and 2D UELs, electron-proton plasmas [37], warm-dense matter [38], double quantum wells [39]) etc. We examine if the pair-densities obtained via the classical-map technique are N -representable and show that N -representability is upheld.

THE CLASSICAL-MAP HYPER-NETTED-CHAIN SCHEME.

Consider an N electron system in a volume V such that $N/V = \bar{n}$, forming a uniform electron liquid in the presence of a neutralizing positive uniform background. The electron eigenfunctions for the self-consistent field problem (Hartree as well as Hartree-Fock models) are simple plane waves $\phi_j(r) = \phi_{\vec{k}\sigma}(\vec{r}) = (\bar{n}/N)^{1/2} \exp(i\vec{k} \cdot \vec{r})\zeta_\sigma$. Here j is an index carrying any relevant quantum numbers including the spin index σ associated with the spin function ζ . Here $\sigma = 1, 2$ or ‘up, down’, specifies the two possible spin states. Some of the vector notation will be suppressed for simplicity, given a uniform liquid which has spherical symmetry in 3D and planar symmetry in 2D. The spin index may also be suppressed where conve-

nient.

The non-interacting pair-distribution function $g^0(r)$

The many-electron wavefunction for non-interacting electrons, as well as for Hartree-Fock (mean-field) electrons is a normalized antisymmetric product of planewaves [40], i.e, a Slater determinant $D(\phi_1, \dots, \phi_j)$ of N -plane waves. Its square is the N -particle density matrix, while the PDF is the two particle density matrix [41]. The latter is obtained by integrating over all but two space coordinates and summing over the $N - 2$ spin variables. At finite T , the N -electron problem needs a very large number $\mathcal{N} > N$ of plane waves as the mean electron occupations in quantum states become fractional. At $T = 0$ all occupation numbers reduce to unity or zero. Then a plane-wave basis set of N functions suffices for the non-interacting problem. In the following we assume Hartree atomic units with $|e| = \hbar = m_e = 1$, where standard symbols are used.

$$g_{\sigma_1, \sigma_2}(\vec{r}_1, \vec{r}_2) = V^2 \Sigma_{\sigma_3 \dots \sigma_N} \int d\vec{r}_3 \dots \vec{r}_N D(\phi_1, \dots, \phi_j). \quad (6)$$

If the spins are anti-parallel, then the non-interacting PDF, $g_{u,d}^0(r)$ is unity for all \vec{r} . Denoting $(\vec{r}_1 - \vec{r}_2)$ by \vec{r} , and $(\vec{k}_1 - \vec{k}_2)$ by \vec{k} , we have, for parallel spins,

$$g_{\sigma, \sigma}^0(\vec{r}) = \frac{2}{N^2} \Sigma_{\vec{k}_1, \vec{k}_2} f(k_1) f(k_2) \left[1 - \exp(i\vec{k} \cdot \vec{r}) \right] \quad (7)$$

$$f(k) = \left[1 + \exp\{(k^2/2 - \mu^0)/T\} \right]^{-1}. \quad (8)$$

Here we have generalized the result to finite T , where the temperature is measured in energy units. Thus the non-interacting PDFs, i.e., $g^0(r)$ are explicitly available at $T = 0$, and numerically at finite T .

$$g_{\sigma, \sigma}^0(r) = 1 - F^2(r) \quad (9)$$

$$F(r) = (6\pi^2/k_F^3) \int f(k) \frac{\sin(kr)}{r} \frac{kdk}{2\pi^2} \quad (10)$$

$$3D, \text{ zero } T, = 3 \frac{\sin(x) - x \cos(x)}{x^3}, \quad x = k_F r. \quad (11)$$

The equations contain the Fermi momentum k_F which is defined in terms of the mean density \bar{n} and the corresponding electron Wigner-Seitz radius r_s . Here we have assumed equal amounts of up and down spins (paramagnetic case) and defined the Fermi wavevector k_F .

$$k_F = 1/(\alpha r_s), \quad r_s = [3/(4\pi\bar{n})]^{1/3}, \quad \alpha = (4/9\pi)^{1/3}. \quad (12)$$

Similar expressions can be developed for the 2D electron layer [34], two coupled 2D-layers [39] and a two-valley 2D layer [42] which are multi-component cases of technological interest, e.g., in the study of metal-oxide field-effect transistors. The method has also been used successfully to obtain the local-field factors of 2D layers at zero and finite- T [43], and for the study of thick 2D layers which are of technological interest [44].

The N -representability of $g^0(r)$ and its classical map

The PDFs $g_{\sigma, \sigma'}^0(r) = 1 - \delta_{\sigma, \sigma'} F(r)$ calculated in the previous section were derived from the Slater determinant $D(\phi_1, \dots, \phi_N)$ and hence manifestly N -representable. At this stage, irrespective of where it came from, we regard $g^0(r)$ as a classical pair-distribution function for particles interacting by a classical pair potential $\beta\mathcal{P}(r)$ where β is the inverse temperature. This is the first step in our classical map, and we may now identify one of the classical particles as being at the origin, without loss of generality, in a classical picture of the PDF. Clearly, for anti-parallel spins, i.e., $\sigma \neq \sigma'$, the pair-potential $\beta\mathcal{P}(r)$ is zero, while it is finite and creates the well-known ‘exclusion hole’ in the PDF of two parallel-spin fermions. Hence $\mathcal{P}(r)$ has been called the ‘Pauli exclusion potential’ and should not be confused with the Pauli kinetic potential that appears in the theory of the kinetic energy functional.

F. Lado was the first to present an extraction of $\beta\mathcal{P}(r)$ for 3D electrons at $T = 0$ using the hyper-netted-chain (HNC) equation and the Ornstein-Zernike (OZ) equation [45]. Only the dimensionless potential, $\beta\mathcal{P}(r)$ is determined from the equations. Although the physical temperature T of the quantum fluid is zero, the temperature of the classical fluid invoked by the map is left undetermined in the ‘non-interacting’ system. The Pauli exclusion potential for 2D electrons at arbitrary T was derived in Ref. [34]. Although the quantum electrons are not interacting via a Coulomb potential, $\beta\mathcal{P}(r)$ becomes a classical manifestation of entanglement interactions which scale as r/r_s , and hence extend to arbitrarily large distances [46]. Assuming that $g^0(r)$ can be expressed as an HNC equation, we have:

$$g^0(r) = \exp[-\beta\mathcal{P}r + h^0(r) - c^0(r)] \quad (13)$$

$$h^0(r) = c^0(r) + \bar{n} \int d\vec{r}' h^0(|\vec{r} - \vec{r}'|) c^0(\vec{r}') \quad (14)$$

$$h^0(r) = g^0(r) - 1. \quad (15)$$

The first of these is the HNC equation, while the second equation is the O-Z relation. These contain the direct correlation function $c^0(r)$ and the total correlation function $h^0(r)$. It should be noted that we have ignored the two-component character of the electron fluid (two spin types) in the equations for simplicity, but the full expressions are given in, say, Ref. [33]. These equations can be solved by taking their Fourier transforms, and the Pauli exclusion potential can be obtained by the inversion of the HNC equation. The ‘Pauli exclusion potential’ $\beta\mathcal{P}(r)$ is given by

$$\beta\mathcal{P}(r) = -\log[g^0(r)] + h^0(r) - c^0(r). \quad (16)$$

The Pauli exclusion potential is a universal function of rk_F or r/r_s . It is long ranged and mimics the exclusion effects of Fermi statistics. At finite T its range is about a

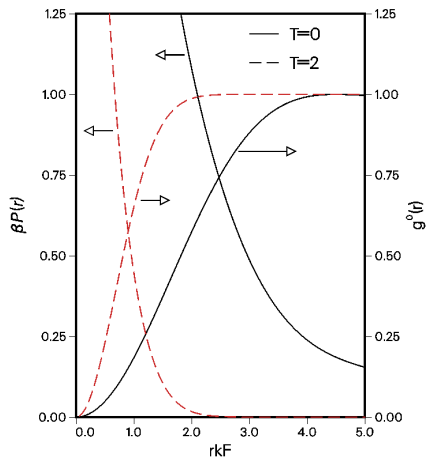


FIG. 1. The exclusion potential, Eq. 16, and the noninteracting PDF, $g_{\sigma,\sigma}^0$ at $t = T/E_F = 0$ (solid line) and at $t = 2$ (dashed line). They are universal functions of r/r_s . The PDF $g_{\sigma \neq \sigma'}^0(r) = 1$ as there is no exclusion effect for $\sigma \neq \sigma'$.

thermal wavelength and is increasingly hard-sphere-like as $r \rightarrow 0$. The Fourier transform $\beta\mathcal{P}(q)$ in 3D behaves as $\sim 1/q$ for small q , and as $\sim c_1/q^2 + c_2/d^4$ for large q .

Plots of $\beta\mathcal{P}(r)$ and $g^0(r)$ for a 3D UEL are given in Fig. 1.

We note that the HNC or MHNC integral equation, together with the OZ equation may be regarded as a transformation where, given the dimensionless pair potential $\beta\phi_{ij}(r)$, the corresponding PDF, i.e., $g_{ij}(r)$ is generated. Similarly, given the $g_{ij}(r)$, HNC inversion is the process which extracts the corresponding $\beta\phi_{ij}(r)$. The value of $g(r)$ for the full range of r , or additional constraints are needed to obtain an unequivocal HNC inversion to extract a valid pair potential [47, 48].

THE INTERACTING SYSTEM AND ITS CLASSICAL MAP

In the previous section we reviewed a classical fluid whose $g^0(r)$ exactly recovers the PDFs of the noninteracting quantum UEL at any density, spin polarization or temperature. From now on, for simplicity we consider a paramagnetic electron gas (equal amounts of up spins and down spins) although spin-dependent quantities will be indicated where needed for clarity. Although the quantum liquid was ‘noninteracting’, the classical map already contains the pair potential $\beta U_{ij} = \beta\mathcal{P}(r)$.

On addition of a Coulomb interaction $\beta V_{ij}(r)$ the total

pair potential becomes

$$\beta U_{ij}(r) = \beta\mathcal{P}(r) + \beta V_{cou}(r). \quad (17)$$

The temperature $T = 1/\beta$ occurring in Eq. 17 is as yet unspecified. In quantum systems the Coulomb interaction is given by the operator $1/|\vec{r}_1 - \vec{r}_2|$ which acts on the eigenstates of the interacting pair. It can be shown (e.g., by solving the relevant quantum scattering equation) that the classical Coulomb interaction, $V_{cou}(r), r = |\vec{r}_1 - \vec{r}_2|$ acquires a diffraction correction for close approach. Depending on the temperature T , an electron is localized to within a thermal de Broglie wavelength. Thus, following earlier work on diffraction corrected potentials, (e.g., in Compton scattering in high-energy physics), or in plasma physics as in, e.g., Minoo et al.,[49] we use a “diffraction corrected” Coulomb potential.

$$V_{cou}(r) = (1/r)[1 - e^{-r/\lambda_{th}}]; \lambda_{th} = (2\pi\bar{m}T_{cf})^{-1/2}. \quad (18)$$

Here \bar{m} is the reduced mass of the interacting electron pair, i.e., $m^*(r_s)/2$ a.u., where $m^*(r_s)$ is the electron effective mass. It is weakly r_s dependent, e.g., ~ 0.96 for $r_s = 1$. In this work we take $m^* = 1$. The “diffraction correction” ensures the correct quantum behaviour of the interacting $g_{12}(r \rightarrow 0)$ for all r_s . The essential features of the classical map are

1. The use of the exact non-interacting quantum PDFs $g_{\sigma,\sigma'}^0(r)$ as inputs.
2. The use of a diffraction corrected Coulomb interaction.
3. The specification of the temperature of the classical Coulomb fluid $T_{cf} = 1/\beta$ as the one that recovers the quantum correlation energy $E_c(r_s)$.

The selection of the classical fluid temperature is a crucial step. This is guided by the Hohenberg-Kohn-Mermin property that the exact minimum free energy is determined by the true one-body electron density $n(r)$. Since we are dealing with a uniform system, the Hartree energy E_H is zero. The exchange energy E_x is already correctly accounted for by the construction of the classical-map $g^0(r)$ to be identical with the quantum $g^0(r)$ at any T or spin polarization. Hence we choose to select the temperature T_{cf} of the classical Coulomb fluid to match the known DFT correlation energy E_c at each r_s at $T = 0$. Since this is most accurately known for the spin-polarized electron liquid, T_{cf} is determined from $E_c(r_s)$ for full spin polarization. A trial temperature is selected and the interacting $g(r, \lambda)$ is determined for various values of the coupling constant λ in the interaction $\lambda V_c(r)$ to calculate a trial E_c at the given r_s from the coupling constant integration. The temperature is iteratively adjusted until the $E_c(r_s, T_{cf})$ obtained from the classical fluid $g(r)$ agrees

with the known quantum $E_c(r_s, T=0)$. Given an electron fluid at $T=0$, the temperature of the classical fluid that has the same E_c is called its *quantum temperature* T_q . This was parametrized as:

$$T_q/E_F = 1.0/(a + b\sqrt{r_s} + cr_s) \quad (19)$$

For the range $r_s = 1$ to 10, T_q/E_F goes from 0.768 to 1.198. The values of the parameters a, b, c are given in Ref. [33].

There is no *a priori* reason that the $n(r)$, i.e., $\bar{n}g(r)$ obtained by this procedure would agree with the quantum $\bar{n}g(r)$, except for the Hohenberg-Kohn theorem that requires $n(r)$ to be the true density distribution when the energy inclusive of the XC-energy is correctly recovered. Many well-known quantum procedures (e.g., that of Singwi et al. [50, 51]) for the PDFs lead to negative $g(r)$ as r_s is increased beyond unity even into the ‘liquid metal’ r_s range.

However, as shown in Refs. [33, 34, 52] and subsequent work, the classical map HNC $g(r)$ provides an accurate approximation to the QMC PDFs where available. Correlations are stronger in reduced dimensions. The classical map for the 2D UEL was constructed using the modified-HNC equation where a hard-sphere bridge function was used, with the hard-sphere radius determined by the Gibbs-Bogoliubov criterion, as prescribed by Lado, Foils and Ashcroft (LFA) [53]. Other workers [35, 36, 54] have examined different parametrizations than our fit form Eq. 19. Sandipan and Dufty [55] examined the connection between the classical map approach and the method of quantum statistical potentials [56, 57] within a grand-canonical formalism. They also proposed using additional conditions (besides the requirement that E_c is reproduced by T_{cf}) to constrain the classical map, recently reviewed by Dorheim et al [58].

Although E_c values at $T=0$ were available when the classical map for the UEL was constructed, no reliable XC-functional (beyond RPA) was available for the finite- T electron liquid. Hence we proposed the use of the equation

$$T_{cf} = (T_q^2 + T^2)^{1/2} \quad (20)$$

as a suitable map for the finite- T UEL. This was based on the behaviour of the heat capacity and other thermodynamic properties of the UEL. Furthermore, using Eq. 20 it became possible to predict the XC-free energy $F_{xc}(r_s, T)$ as well as the finite- T PDFs of the UEL at arbitrary temperatures and spin polarizations. These were found to agree closely with the $F_{xc}(r_s, T)$ and PDFs resulting from the Feynman Path Integral Monte Carlo (PIMC) simulations reported 13 years later by Brown et al. [59]. The Brown et al data have been used by Liu and Wu [54] to construct a direct fit of a T_{cf} that avoids the model used in Eq. 20, by using temperature dependent parameters a, b and c in Eq. 19. The PIMC data

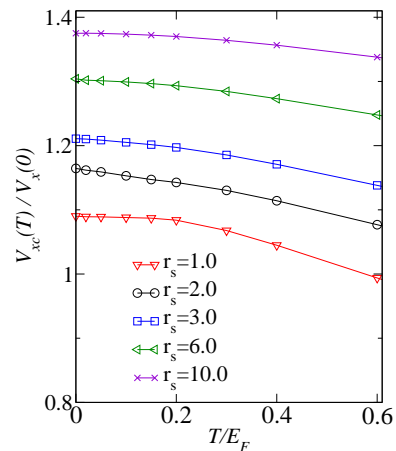


FIG. 2. (Color online) Finite- T exchange and correlation free energy $f_{xc}(r_s, T)$ per electron (Hartrees) versus the reduced temperature $t = T/E_F$ in units of the Fermi energy. The symbols are the path integral Monte Carlo (PIMC) data of Brown et al. Ref. [59] as given in Ref. [60]. The continuous lines are from the classical-map HNC procedure parametrized by Perrot and Dharma-wardana, Ref. [52]. The temperature range $t < 1$ is the region of interest for WDM studies. The thermal-XC corrections to the $T=0$ XC-functional are most important near $t \simeq 0.5$ and then decrease with increasing T .

have been parametrized by Karasiev et al, Ref. [60] and further improved by Groth et al. Calculations of F_{xc} using the finite T parametrization given by Perrot and Dharma-wardana [52] are compared with the Feynman path results in Fig. 2. The parametrization of the finite- T XC free energy given by Perrot et al. [52], Iyatomi and Ichimaru, and subsequent parametrizations incorporates the high- T Debye-Hückel limit of F_c , the high- T behavior of $F_x(T)$, as well as the behaviour at the $T=0$ limit. Groth, Dornheim et al. [61] presented a new *ab initio* parametrization of $F_{xc}(r_s, T)$ using accurate data from recently developed finite- T QMC methods [58].

N -representability of the interacting $g(r)$ of the classical map.

The conditions $n(r) = \bar{n}g(r) > 0$, and $\int n(\vec{r})d\vec{r} = N$ are always satisfied by the classical map procedure. Furthermore, the classical map becomes increasingly exact as $t = T/E_F$ is increased and electrons become increasingly classical.

We present two arguments to conclude that the $g(r)$ of the interacting UEL obtained by the classical map procedure is N -representable.

(1)**Argument based on the HNC equation being an N representability conserving transformation.** Once the $g^0(r)$ of the quantum fluid is evaluated we consider a classical fluid which has the same $g^0(r)$. The non-interacting $g^0(r)$ and the corresponding $n^0(r) = \bar{n}g^0(r)$

of the classical fluid are generated from the homogeneous density \bar{n} by a transformation where the origin of coordinates is moved to one of the particles. The corresponding transformation of the density profile is written as:

$$n^0(r) = \mathcal{T}_0(r)\bar{n} \quad (21)$$

$$\mathcal{T}_0(r) = \exp[\beta\mathcal{P}(r) + h^0(r) + c^0(r)]. \quad (22)$$

$$(23)$$

The so generated $n^0(r)$ is N -representable by its construction from a Slater determinant. Then, in a next step the interacting $g(r)$ is generated from the N -representable non-interacting $g^0(r)$ by a transformation which can be written as:

$$g(r) = \mathcal{T}_1(r)g^0(r) \quad (24)$$

$$\begin{aligned} \mathcal{T}_1(r) &= e^{\beta V_{cou}(r) + \{h(r) - h^0(r)\} + \{c(r) - c^0(r)\}} \\ &= \exp[\beta\{V_{cou}(r) + V_{pmf}(r)\}]. \end{aligned} \quad (25)$$

In effect, the uniform density \bar{n} has been transformed (by a selection of the origin of coordinates, and by switching on the Coulomb interaction) by a single composite transformation $\mathcal{T} = \mathcal{T}_1\mathcal{T}_0$ with its components acting one after the other.

In equation 25 we use $V_{pmf}(r)$ to indicate the correlation correction to the potential of mean force; this is expected to be a well-behaved function. The diffraction corrected classical Coulomb potential $V_{cou}(r)$ has a finite-value at $r = 0$, and not singular, unlike the point-Coulomb potential $1/r$. Hence we may regard the above transformation as being mathematically equivalent to a type of smooth coordinate transformation of \vec{r} to another variable \vec{s}

$$d\vec{s} = \mathcal{T}(r)\bar{n}d\vec{r} = n(r)d\vec{r}. \quad (26)$$

That is, the initial planewave states $(\bar{n}/N)^{1/2} \exp(i\vec{k} \cdot \vec{r})$ are transformed to a new set $(n(\vec{r})/N)^{1/2} \exp(i\vec{q} \cdot \vec{s}(r))$. It is easily shown that they form a mutually orthogonal complete set. For instance, consider the initial planewave state used in the Slater determinant, i.e., $\phi_j(\vec{r}) = \phi_k(\vec{r})$ and consider its transformed state $\tilde{\phi}_k(\vec{r})$ given below:

$$\phi_k(\vec{r}) = (\bar{n}/N)^{1/2} \exp(i\vec{k} \cdot \vec{r}) \quad (27)$$

$$\tilde{\phi}_k(\vec{r}) = (n(\vec{r})/N)^{1/2} \exp(i\vec{k} \cdot \vec{s}(\vec{r})). \quad (28)$$

We regard \vec{k} as an arbitrary k -vector and hence it is sufficient to transform \vec{r} , while the theory can also be constructed entirely in k -space in an analogous manner. The transformed wavefunctions $\tilde{\phi}_k(\vec{r})$ have the following properties:

$$\int \tilde{\phi}_{k'}^*(\vec{r}) \tilde{\phi}_k(\vec{r}) d\vec{r} = \int \frac{n(\vec{r})}{N} e^{i(\vec{k}' - \vec{k}) \cdot \vec{r}} d\vec{r} \quad (29)$$

$$= \frac{1}{N} \int \exp\{i(\vec{k}' - \vec{k}) \cdot \vec{s}\} \frac{d\vec{s}}{N} \quad (30)$$

$$= \frac{(2\pi)^3}{N} \delta^3(\vec{k}' - \vec{k}). \quad (31)$$

Furthermore,

$$\int \tilde{\phi}_k^*(\vec{r}) \tilde{\phi}_k(\vec{r}') \frac{d\vec{k}}{(2\pi)^3} = \frac{\delta^3(\vec{r} - \vec{r}')}{N}. \quad (32)$$

Hence the transformed functions $\tilde{\phi}_k(\vec{r})$ form a complete orthogonal set. This implies that the initial Slater determinant $D(\phi_{k_1}, \dots, \phi_{k_N})$ of the noninteracting electron system transforms to the determinant $D(\tilde{\phi}_{k_1}, \dots, \tilde{\phi}_{k_N})$ of the interacting system, explicitly showing the N -representability of the $n(r) = \bar{n}g(r)$ obtained via the classical map which consists of the application of the two transformations $\mathcal{T}_1\mathcal{T}_0$. Furthermore, the transformations commute, in the sense that one may first apply *only* the diffraction corrected Coulomb potential to non-interacting fermions to generate a $g^c(r)$ for a Coulomb fluid, and then apply the Pauli exclusion potential to generate the fully interacting classical map inclusive of exchange-correlation effects, or *vice versa*. This is equivalent to iterating the HNC equations from the non-interacting state via two different paths, and indeed the two different procedures, $\mathcal{T}_1\mathcal{T}_0$ and $\mathcal{T}_0\mathcal{T}_1$ lead to the same final $g(r)$.

What if a phase transition, e.g., a Wigner crystallization, intervenes in passing from the non-interacting to the interacting system? The CHNC procedure for a uniform system will produce the best interacting fluid state (an upper bound to the ground-state energy) and not the lower-energy Wigner crystal state. This is still consistent with the variational principle and N -representability.

The above analysis confirms the N -representability of the pair-densities of the interacting uniform electron liquid generated by the classical map presented here.

(2) Argument based on the N -representability of the QMC density.

The diffusion quantum Monte Carlo (DQMC) calculations use a Slater determinant together with Jastrow factors, and hence the DQMC procedure is based on an explicit many-body wavefunction whose variation produces a minimum energy and a corresponding $E_c(r_s)$. Hence its two-particle reduced density matrix, i.e., the electron-electron PDF is N -representable; the correlation energy E_c associated with the N -representable two-body density is the correlation contribution to the best approximation to the energy minimum as per Hohenberg-Kohn theorem, since the minimum is achieved only for the true density. The CHNC electron-electron PDFs agrees with the DQMC- $g(r)$ with *no attempt at fitting* the PDFs. The only input is the single number $E_c(r_s)$ at each density introduced via the classical temperature T_{cf} - a classical kinetic energy. Thus, both the electron density $\bar{n}g(r)$ and its E_{xc} agree with those of the N -representable density $\bar{n}g_{DQMC}(r)$ as well as the energy E_{xc} from DQMC. Hence we conclude that the CHNC $n(r)$ is as N -representable as the DQMC procedure.

It should be noted that the classical pair potential

$U(r) = \mathcal{P}(r) + V_{cou}(r)$ may be used in a classical molecular dynamics simulation to generate the interacting $g(r)$ instead of using the HNC equations. Such a procedure can reveal crystal ground states and go beyond the liquid-model inherent in the usual HNC equations. It is also possible to generate the dynamics of fluid states, e.g., determine $S(k, \omega)$ by a classical simulation. However, the Pauli exclusion interaction is really a kinematic quantum effect and not a true ‘interaction’. It is not known at present whether such a classical map $S(k, \omega)$ agrees in detail with the quantum $S(k, \omega)$ for an interacting electron fluid.

CHNC METHOD FOR SYSTEMS OF INTERACTING ELECTRONS AND IONS

In this section the UEL model is extended to two interacting subsystems, namely electrons and ions, or possibly for electrons and holes. The application of the CHNC method to coupled electron-ion system will be illustrated by calculations of hydrogen plasmas where the CHNC results are compared with NPA calculations, as well as recent QMC, PIMC, DFT-MD and other N-center simulation methods. The CHNC, NPA and Quantum-simulation methods are in good agreement. This agreement is the basis of our second argument for the N -representability of the pair-densities obtained from the CHNC method.

Consider the two coupled density functional equations of the NPA, viz., Eqs. 5. As shown in the appendix to Ref. [19] these equations for $n(r), \rho(r)$, when applied to classical particles reduce to classical Kohn-Sham equations which are Boltzmann like distributions. In the classical case they can be reduced to two coupled HNC-like equations for the electrons and ions. The HNC equation (with or without a Bridge term) for the electrons when replaced by their classical map gives the CHNC equation which now includes an electron-ion contribution to the potential of mean force. Similarly, the HNC-like equation for the ions will contain contributions from the electrons. That is, the electron screening of the ions, or ion screening of the electrons is controlled by the CHNC equations, while only the basic pair interactions are needed. If the particles are in the quantum regime, a Pauli-exclusion potential is needed, be it for electrons, or for protons (or holes in semiconductor applications).

As an example, we take a system of ions of mean charge \bar{Z} , mass M , with a mean density $\bar{\rho}$ interacting with a neutralizing system of electrons at a mean density $\bar{n} = \bar{Z}\bar{\rho}$. The electron mass is unity in atomic units. For simplicity we assume that there is just one kind of ion, and that $\bar{Z} = 1$ as for a hydrogenic system. We denote the ion species by $p = H^+$. The coupled CHNC equations are given in Eq. 33 and in Refs. [37, 38]. They are discussed below.

The densities $\bar{\rho}$ and \bar{n} are equal since the ion charge $\bar{Z} = 1$. Consider a fluid of total density n_{tot} , with three species, electrons of two types of spin, $n_s = \bar{n}/2$ for $s = 1, 2$ for the two spin species, and $s = 3, n_3 = \bar{\rho}$ for the ions, denoted here as ‘p’. The physical temperature is T , while the classical-fluid temperature of the electrons, $T_{cf} = T_{ee} = 1/\beta_{ee}$, with $1/\beta_{ee} = \sqrt{(T^2 + T_q^2)}$. For the ion $p = H^+$, no quantum correction is usually needed and $T_{pp} = 1/\beta_{pp}$ is T . Otherwise an ion-quantum temperature T_{qp} is defined as before, using Eq. 19, but using the Fermi Energy E_{Fp} of the ions (or holes). If the densities are those typical of stellar densities, then the calculation will automatically be for quantum hydrogen ions as appropriate. Normally, treating the positively charged counter particles of the electrons quantum mechanically is not needed except in semi-conductor structures.

Thus the classical map converts the system with the physical temperature T into a system with multiple temperatures associated with the different subsystems T_{ee}, T_{pp} . But the cross subsystem temperature T_{ep} is not easily defined as there is no uniform density or specific Fermi energy associated with the cross-interactions. It can however be unambiguously extracted from an NPA calculation or constructed from a suitable physical model, as discussed below. So, using $T_{ij} = 1/\beta_{ij}$ and ϕ_{ij} for the interparticle temperatures and pair-potentials, the coupled CHNC and OZ equations for the PDFs are:

$$g_{ij}(r) = e^{[-\beta_{ij}\phi_{ij}(r) + h_{ij}(r) - c_{ij}(r) + B_{ij}(r)]} \quad (33)$$

$$h_{ij}(r) = c_{ij}(r) + \sum_s n_s \int d\mathbf{r}' h_{i,s}(|\mathbf{r} - \mathbf{r}'|) c_{s,j}(\mathbf{r}') \quad (34)$$

The pair potential $\phi_{ij}(r)$ between electrons is just the diffraction corrected Coulomb potential $V_{cou}(r)$ added to the Pauli exclusion potential which vanishes as the de Broglie radius of the particles becomes negligible in approaching the classical regime. The interaction between two ions is also a Coulomb potential with a diffraction correction with a very small length scale ($\sim 1/\sqrt{M}$) due to the mass M of the ions.

The HNC is sufficient for the uniform 3-D electron liquid for a range of r_s , up to $r_s = 50$, as shown previously [52]. But the bridge term is important for the ions at high compressions and low temperatures. Hence we neglect the e-e bridge corrections in this study, but retain them for ions.

The construction of $\beta_{ep}, \phi_{ep}(r)$ requires attention. Only the product, $\beta_{ep}\phi_{ij}(r)$ is unambiguously available from the theory, and that is necessary and sufficient for CHNC calculations. However, simple electron-ion interaction models may also be used. Thus Bredow et al [38] examined the applicability of a very simple electron-ion interaction and a simple model for the inter-subsystem

temperature of the two-temperature classical map.

$$\phi_{ep}^0(r) = U(r)\{1 - \exp(-r/\lambda_{ep})\}, \quad (35)$$

$$U(r) = (-\bar{Z}/r)f(r), \quad f(r) = 1. \quad (36)$$

$$\lambda_{ep} = (2\pi\bar{m}T_{ep})^{-1/2}, \quad \bar{m} = 1., \quad (37)$$

$$T_{ep} = (T_{ee}T_{pp})^{1/2}. \quad (38)$$

The e-p de Broglie length λ_{ep} moderates the $r \rightarrow 0$ behaviour of the electron-proton interaction. The latter includes a pseudopotential $U(r)$ where the form factor $f(r)$ is set to one for the linear-response regime. For ions with a bound core of radius r_c , the form factor can be chosen to have the Heine-Abarankov form. In such cases the diffraction correction becomes irrelevant.

Equation 38 for T_{ep} as a geometric mean of the inter-subsystem temperatures is justifiable in the larger- r or small- k limit using compressibility sumrule arguments [62, 63]. However, for small- r , binary collisions dominate and the ansatz becomes less valid. Furthermore the electron density near the nucleus is large, and the effective T_{ee} increase from the bulk value. Hence a single T_{ep} is not strictly possible but found to work quite well, as shown below. The ion-ion PDF is insensitive to the choice of T_{ep} , and hence the model, Eq. (35), proves to be very convenient.

We display the results from the simple model, Eq. 35 in Fig. 3 and compare them with the results from NPA calculations as well as with highly computer-intensive QMC simulations by Liberatore et al [64]. Liberatore et al assume a linear-response form for the proton-electron interaction following the Hammerberg-Ashcroft model of 1974 [65]. Such a model is normally questionable for protons in an electron gas, as the proton-electron interaction is highly nonlinear [66, 67]. A calculation inclusive of all non-linear effects is available from the NPA model, and displayed in Fig. 4(a) for a single proton, confirming that linear-response is accurate at this density. Figure 3 shows that the NPA and CHNC agree accurately with each other and with quantum simulations. While the non-linear CHNC procedure gives good agreement with the QMC results of g_{pp} , bridge corrections are needed for the form of the ion-ion pair potential used in the NPA, when excellent agreement is obtained, both for the positions of the peaks and the peak heights. The Gibbs-Bogoliubov-LFA criterion determines $\eta = 0.475$ for this ~ 30 -times compressed hydrogen fluid. The g_{ee} and g_{ep} are insensitive to bridge corrections. However, as expected, the accuracy of g_{ep} depends on the choice of $\beta_{ep}\phi_{ep}(r)$. In Fig. 4(b) we see that the ansatz given by Eq.(35) works well even half-way into the Wigner-Seitz (WS) sphere of the electron with the WS radius $r_s = 0.4473$. Hence the model is quite accurate for equation of state, transport and other calculations of compressed hydrogen.

The assumptions in Eq. 35. that $T_{ep} = \sqrt{T_{ee}T_{ii}}$, $\phi_{ep} = Z\{1 - \exp(-r/\lambda)\}/r$, can be avoided if NPA inputs can be used. For instance, in Ref. [37] the free-electron

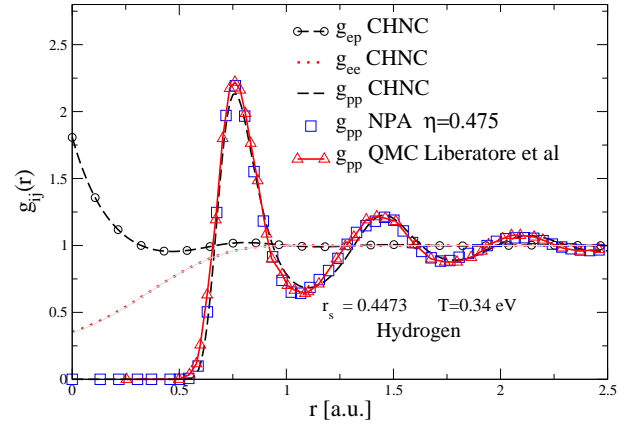


FIG. 3. Pair distribution functions $g_{ij}(r)$, $i, j = e, p$ using the simple CHNC model T_{ep}, ϕ_{ep} from Eq. 35, from the NPA, and from QMC (Liberatore *et al.* [64]), for fully ionized hydrogen. The ion density is $\bar{\rho} = 1.8 \times 10^{25} \text{ cm}^{-3}$ (i.e., ~ 350 times the density of solid hydrogen) with $T = 0.34 \text{ eV}$. The NPA, CHNC and QMC agree very well for g_{pp} when Bridge corrections specified by the hard-sphere packing fraction η are included in the NPA. See Fig. 4 for more details on g_{ep} .

NPA density $n(r \rightarrow 0)$ was used to fix λ_{ep} . A more complete approach is also possible. Thus, if the free-electron density increment around one H^+ ion as calculated from the NPA is $\Delta n_{npa}(r)$, then we define the $g_{ep}[\text{one } H^+](q)$ as follows and invert it by the HNC equation to obtain the effective e-p potential $\beta_{ep}\phi_{ep}$.

$$h_{ep}[\text{one } H^+](q) = \Delta n_{npa}(q, T)/\bar{n} \quad (39)$$

$$g_{ep}(r) = 1 + h_{ep}(r) = 1 + \Delta n_{npa}(r)/\bar{n} \quad (40)$$

$$\beta_{ei}\phi_{ep}(r) = \text{hnc inversion of: } g_{ep}(r) \quad (41)$$

In Eq. 41 we imply that the $g_{ep}(r)$ is now interpreted as a classical PDF in a system containing protons and electrons. It is HNC-inverted to obtain the classical pair-potential $\beta_{ep}\phi_{ep}(r)$ in a manner analogous to the extraction of the Pauli potential from $g_{ee}^0(r)$. However, in the regime of high compressions, the model of Eq. 35 seems to be sufficient.

While the NPA and CHNC calculations agreed with the QMC results of Liberatore et al in the linear-response regime, we show that similar agreement is found in regimes where linear response does not hold. In Fig. 5 we show that the PDFs obtained using our single-center approaches agree very well with highly computer intensive quantum simulations, e.g., those of Morales et al [68] using coupled electron-ion Monte Carlo calculations. The $g_{pp}(r)$ of such quantum simulations are limited by the box size, while the NPA calculations capture the effect of many Friedel oscillations in the potentials. Our results imply that the ion-ion correlation functionals used in the single-center NPA method to incorporate many-ion effects are successful. This has of course been verified in many other calculations during past decades,

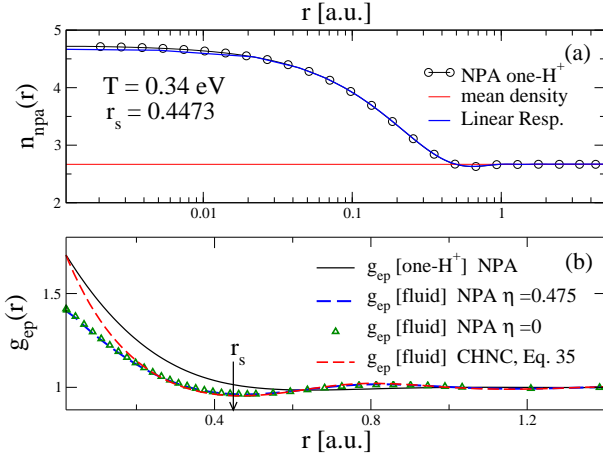


FIG. 4. (a) The free-electron density $n_{\text{npa}}(r)$ calculated from the NPA model at a proton in a hydrogen plasma, $T = 0.34$ eV, with an ion density of $\bar{\rho} = 1.8 \times 10^{25} \text{ cm}^{-3}$, i.e., $r_s = 0.4473$. At this high density linear-response theory (dashed curve) is accurate. (b) The density displacement can be used to define $g_{\text{ep}}(r)$ for the one-proton system and its generalization to the fluid. Results for g_{ep} obtained from a simple model of Eq. 35 within the CHNC, and calculations from the NPA for hydrogen fluid using the MHNC equation are displayed.

even with respect to complex fluids like warm dense carbon, silicon etc., where there are covalent bonding effects as well [22, 23]. A similar verification is available in the context of ion-dynamical calculations [69, 70]. The NPA and CHNC methods are not limited by the Born-Oppenheimer approximation, as the static effects of the electron-nuclear coupling can be incorporated in the electron-ion correlation functionals [71].

The quantum simulation method used by Morales et al is described by them as “a QMC based ab initio method devised to use QMC electronic energy in a Monte Carlo simulation of the ionic degrees of freedom.... Specifically, the use of twist averaged boundary conditions (TABCs) on the phase of the electronic wave function, together with recently developed finite-size correction schemes, allows us to produce energies that are well converged to the thermodynamic limit with 100 atoms”. More detailed calculations using CHNC, NPA, and comparisons of the resulting thermodynamic data (calculated from the PDFs using coupling constant integrations) will be taken up elsewhere.

SYSTEMS WHERE ALL PARTICLES ARE IN THE QUANTUM REGIME

If both subsystems, viz., ions and electrons are in the quantum regime, this poses no additional difficulty for the CHNC method. However, in practice, such corrections in the liquid state are possible only under extreme

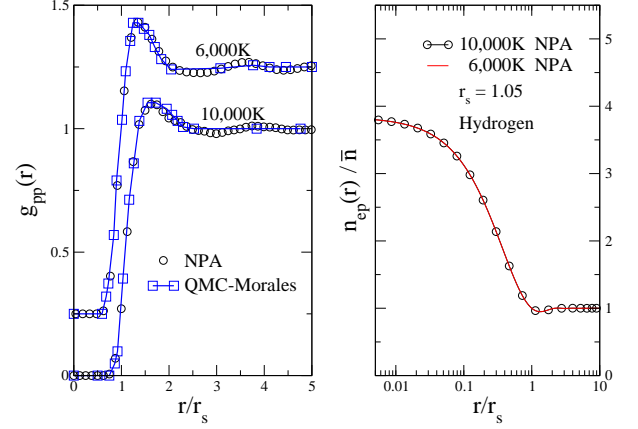


FIG. 5. (b) The fractional free-electron density $n_{\text{npa}}(r)/\bar{n}$ or g_{ep} at a single proton calculated from the NPA model at a proton in a hydrogen plasma at $r_s = 1.05$. This is effectively unchanged between $T=6,000$ and $10,000$ K. (b) The NPA density displacement can be used to define a pseudopotential for the one-proton system and the fluid g_{pp} is calculated using an ion-correlation functional which reduces to the HNC diagrams, as the Bridge corrections are negligible in this case. Results agree closely with the coupled electron-ion quantum Monte Carlo simulations of Morales et al [68] which are however limited by the size of the simulation box. Only the case $r_s = 1.05$ is shown.

compressions, even for hydrogen, and such compressions are only available in astro-physical settings.

On the other hand, in electron-hole systems as found in semiconductor materials, the quantum nature of both types of particles must be included as the hole masses are usually within a factor of ten of the electron mass. Furthermore, if the electrons and holes are confined in two quantum wells separated by a thin insulating barrier, the spontaneous recombination of electrons and holes is suppressed. Such systems can be fabricated and are known as double quantum wells (DQWs) where the electrons and holes occupy the the lowest subband in each well and form two interacting but spatially separated 2-D electron fluids. Properties of such DQWs in the symmetric case, (i.e., for the case where the electron and hole masses m_e, m_h , well widths w_e, w_h , layer dielectric constants and temperatures are equal) has already been studied using the CHNC method [39]. However, in typical GaAs-GaAl_xAs_{1-x} DQWs, the electron and hole masses are, typically, 0.067 and 0.335, respectively, while the material dielectric constant ϵ is taken as ~ 12.9 for the whole structure since the aluminum alloy content x is small. The barrier dielectric constant is typically about 12.62. The effective Bohr radius is given by $a_B^* = \hbar^2 \epsilon / (m_0 e^2 m_s^*)$ where m_0 is the free-electron mass while m_s^* is the effective mass of the species ‘s’. Typical well widths w

TABLE I. Characteristic quantities for electrons and holes in a typical GaAs/GaAlAs in a double quantum well structure. These are examples for 2-dimensional warm dense matter states. The material dielectric constant $\epsilon=12.9$ for both layers separated by an AlAs barrier of 10 nm width and held at a temperature $T = 5K$. Each layer has its effective Bohr radius and effective Hartree unit. So r_s, E_F etc., are expressed in the respective effective units. The classical plasma coupling parameter $\Gamma = 1/(r_s T_{cf})$. for each classical fluid is given.

item	electron layer	hole layer
Particle density (cm^{-2})	4×10^{11}	4×10^{11}
Effective mas $m_s^* = m_s/m_0$	0.0670	0.3350
Layer width (nm)	15.00	20.00
Effective r_s	2.768	13.84
Effective E_F	0.1304	0.5218×10^{-2}
degeneracy parameter T/E_F	0.3015	1.508
Classical fluid temp. T_{cf}/E_F	1.966	2.188
Inverse de Broglie Length	1.180	0.1807
Plasma coupling parameter Γ	1.408	6.327

and barrier widths are 10-30 nm. Given these material properties, a DQW with equal densities of electrons and holes at a temperature of even 5K is found to be a two component interacting partially degenerate system where the r_s, E_F values, and hence the degeneracies are widely different (see Table 1. In fact, these DQWs provide excellent laboratory examples of 2-dimensional interacting warm dense matter. They contain four interacting subsystems as the electrons, and holes are spin 1/2 fermions for GaAs/GaAlAs DQWs, but there is no exchange interaction between particles in separate layers. Such DQWs can be made up of two electron layers, two hole layers, or an electron layer coupled to a hole layer. For more computational details, see Ref. [39].

These systems are of great interest in nanostructure physics as the transport properties, plasmon dispersion, energy relaxation etc., depend on the corresponding structure factors and local-field corrections which enter into response functions and effective potentials. All such quantities can be extracted from CHNC calculations [33, 39]. Currently, the CHNC technique is the only method available for treating such systems at arbitrary layer degeneracies, spin polarizations, and arbitrary effective masses at zero to finite temperatures. The pair-distribution functions for the spin unpolarized e-h DQW system described in Table 1 are displayed in Fig. 6. Unfortunately, QMC or other microscopic calculations for such systems are believed to be too prohibitive at present, and no comparisons are available.

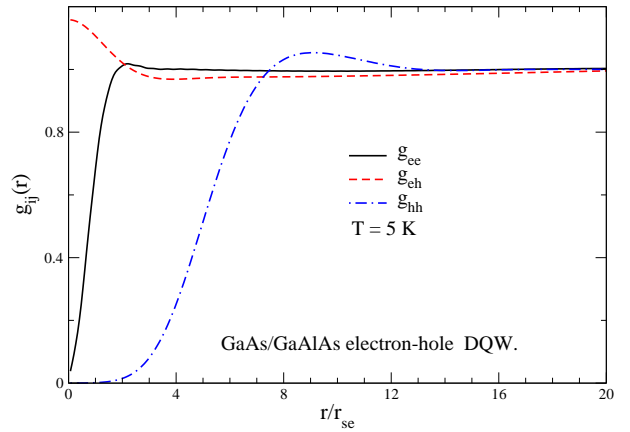


FIG. 6. The e-e, e-h and h-h pair distribution functions $g(r)$ for an electron layer interacting with a hole layer in a GaAs/GaAlAs double quantum well maintained at 5K. The x -axis is in units of the electron Wigner-Seitz radius $r_{se} = 2.768$ in units of the effective electron atomic unit of length (materials details are given in Table 1). This is an example of quasi two-dimensional warm dense matter, albeit at 5K.

The N -representability and v -representability of CHNC densities for electron-ion systems

The N -representability of the electron-electron $g_{ee}(r)$ obtained from the CHNC method for electron-ion systems needs to be examined. This too can be approached as in the previous section. It appears that N -representability is preserved in this case too, where we have merely made the electrons to interact with the ‘external potential’ of the ions which is, however, self-consistently adjusted in the two component problem, with no invoking of the Born-Oppenheimer approximation. The BO corrections come through the electron-ion correlation potentials (HNC-like diagrams) contained in the HNC equation describing the $g_{ep}(r)$ pair distribution function [71].

We may also note that the v -representability of the densities generated by CHNC, or via the NPA can be treated rather easily since we are dealing entirely with Coulombic systems and spherical charge densities. For such systems, Kato’s theorem [72] applies, and the methods based on spherical densities can be used [73, 74].

CONCLUSION

A review of the classical map hyper-netted chain procedure, which is a way of side stepping the construction of a quantum kinetic energy functional for density functional theory is presented. A proof of the N -representability of the classical map, and some plausibility arguments for N -representability are given. The application of the CHNC method to general electron-ion

systems is reviewed. Computationally demanding quantum systems like warm dense matter become numerically much simpler within the CHNC method. It can also be used with the HNC procedure replaced by classical MD simulations. Thus, within certain limits, entirely classical calculations which are very rapid and scale as the zeroth power of the number of particles may be possible for a wide class of quantum problems.

The author thanks Professors Sam Trickey and Jim Dufty for raising the question of the N -representability of the CHNC procedure at the CECAM workshop at Lausanne, Switzerland, 2019.

* Email address: chandre.dharma-wardana@nrc-cnrc.gc.ca

- [1] A. J. Coleman, Rev. Mod. Phys. **35**, 668 (1963).
- [2] R. Erdahl and V. H. Smith Jr., Eds., *Density Matrices and Density Functionals: Proceedings of the A. John Coleman Symposium* (Reidel, Boston, 1987).
- [3] P. Hohenberg and W. Kohn, Phys. Rev., **136**, B864 (1964).
- [4] W. Kohn and L. J. Sham, Phys. Rev. **140**, A1133 (1965).
- [5] R. M. Dreizler and E. K. U. Gross, *Density Functional Theory*, (Springer, Berlin, 1990).
- [6] F. Perrot and M. W. C. Dharma-wardana, Phys. Rev. A **30**, 2619 (1984).
- [7] N. D. Mermin, Phys. Rev. B **1**, 2362 (1970).
- [8] K. Capelle and G. Vignale, Phys. Rev. Lett, **86** 5546 (2001).
- [9] Louis Garrigue, arXiv:1906.03191v1 [math-ph] (2019).
- [10] Joseph E. Mayer, Phys. Rev. **97** 1579 (1955).
- [11] M. Levy, Phys. Rev. A, **26**, 1200, (1982).
- [12] D. A. Mazziotti, Phys. Rev. Lett. **108**, 263002 (2012).
- [13] Y. A. Wang and E. A. Carter, Chapter 5 of *Theoretical Methods in Condensed Phase Chemistry*, in book series of *Progress in Theoretical Chemistry and Physics*, edited by S. D. Schwartz, pp. 117-184 (Kluwer, Dordrecht, 2000).
- [14] V. V. Karasiev, T. Sjöström, and S. B. Trickey, Phys. Rev. B **86**, 115101 (2012).
- [15] T. G. White, S. Richardson, B. J. B. Crowley, L. K. Pattison, J. W. O. Harris, and G. Gregori, Phys. Rev. Lett. **111**, 175002 (2013).
- [16] Jouko Lehtomäki, Ilja Makkonen, Miguel A. Caro, Ari Harju, and Olga Lopez-Acevedo, J. Chem. Phys. **141**, 234102 (2014). [<http://dx.doi.org/10.1063/1.4903450>].
- [17] J. Cl  rouin Gr  gory Robert, Philippe Arnault, Christopher Trickey, Joel D. Kress, and Lee A. Collins Phys. Rev. E **91** 011101(R), (2015).
- [18] L. Dagens, J. Phys. (Paris) **36**, 521 (1975).
- [19] M. W. C. Dharma-wardana and F. Perrot, Phys. Rev. A **26**, 2096 (1982).
- [20] E. K. U. Gross, and R. M. Dreizler, *Density Functional Theory*, NATO ASI series, **337**, p 625, Plenum Press, New York (1993).
- [21] F. Perrot and M.W.C. Dharma-wardana, Phys. Rev. E. **52**, 5352 (1995).
- [22] M. W. C. Dharma-wardana and F. Perrot, Phys. Rev. Lett., **65**, 76 (1990).
- [23] M. W. C. Dharma-wardana, Contrib. Plasma Phys. **58** 128-142 (2018).
- [24] M. Ishitobi and J. Chihara, J. of Physics: Condensed matter, **4** 3679 (1992).
- [25] J. A. Anta and A. A. Louis, Phys. Rev. B **61**, 11400 (2000).
- [26] Hong Xu and J. P. Hansen, Physics of Plasmas **9**, 21 (2002).
- [27] J. Chihara, Progress in Theoretical Physics **72**, 940 (1984).
- [28] G. Kresse and J. Furthm  ller, Phys. Rev. B **54**, 11169 (1996).
- [29] X. Gonze and C. Lee, Computer Phys. Commun. **180**, 2582-2615 (2009).
- [30] M. Levy and HuiOu-Yang, Phys. Rev. A **38**, 625 (1988).
- [31] V. Karasiev, S. Trickey, and F. Harris, J. Comput. Aided Mater. Des. **13**, 111 (2006).
- [32] C. J. Umrigar and Xavier Gonze, Phys. Rev. A **50**, 3827 (1994).
- [33] M. W. C. Dharma-wardana and F. Perrot, Phys. Rev. Lett. **84**, 959 (2000).
- [34] Fran  ois Perrot and M. W. C. Dharma-wardana, Phys. Rev. Lett. **87**, 206404 (2001).
- [35] C. Bulutay and B. Tanatar, Phys. Rev. B **65**, 195116 (2002).
- [36] Chieko Totsuji, Takashi Miyake, Kenta Nakanishi, Kenji Tsuruta and Hiroo Totsuji, J. Phys.: Condens. Matter **21** 045502 (2009).
- [37] Dharma-wardana, M. W. C.; and Perrot, F.; Phys. Rev. B **66**, 014110 (2002).
- [38] R. Bredow, Th. Bornath, W.-D. Kraeft, M.W.C. Dharma-wardana and R. Redmer Contributions to Plasma Physics, **55**, 222-229 (2015).
- [39] M. W. C. Dharma-wardana, D. Neilson and F. M. Peeters, Phys. Rev. B **99**, 035303 (2019). <https://arxiv.org/abs/1901.00895>
- [40] G. D. Mahan, *Many particle Physics*, Sec. 5.1, Plenum Publishers, New York (1981).
- [41] G. F. Giuliani et al., *Quantum Theory of the Electron Liquid*, Appendix 4, Cambridge University Press (2005).
- [42] M. W. C. Dharma-wardana and F. Perrot, Phys. Rev. B **70**, 035308 (2004).
- [43] M. W. C. Dharma-wardana and Fran  ois Perrot, Europhys. Letters, **63**, 660 (2003).
- [44] M. W. C. Dharma-wardana, Phys. Rev. B **72**, 125339 (2005).
- [45] F. Lado, J. Chem. Phys. **47**, 5369 (1967).
- [46] M. W. C. Dharma-wardana, J. Phys. Conf. Ser. **442**, 012030 (2013).
- [47] Dharma-wardana, M. W. C. and Aers, G. C., Phys. Rev. Lett. **56**, 1211 (1986).
- [48] Yaakov Rosenfeld and Gerhard Kahl, J. Phys.: Condens. Matter **9** L89, (1997).
- [49] H. Minoo, M. M. Gombert, and C. Deutsch, Phys. Rev. A **23**, 924 (1981).
- [50] Singwi, M. P. Tosi, R. H. Land, and A. S  lander, Phys. Rev. **176**, 589 (1968).
- [51] P. Vashista and K. S. Singwi, Phys. Rev. B **6**, 875 (1972).
- [52] F. Perrot and M. W. C. Dharma-wardana, Phys. Rev. B **62**, 16536 (2000); *Erratum*: **67**, 79901 (2003); arXiv-1602.04734.
- [53] F. Lado, S. M. Foiles and N. W. Ashcroft, Phys. Rev. A **28**, 2374 (1983).
- [54] Yu Liu and Jianzhong Wu, J. Chem. Phys **141**, 064115 (2014).
- [55] J. Dufty, and S. Dutta, Phys. Rev. E **87**, 032101 (2013).

- [56] G. Kelbg, Ann. Phys. **467**, 219 (1963).
- [57] A. V. Filinov, V. O. Golubnychiy, M. Bonitz, W. Ebeling, and J. W. Dufty, Phys. Rev. E **70**, 046411 (2004).
- [58] Tobias Dornheim, Simon Groth, Michael Bonitz Physics Reports, **744**, 1-86 (2018), <https://doi.org/10.1016/j.physrep.2018.04.001>.
- [59] E. W. Brown, J. L. DuBois, M. Holzmann and D. M. Ceperley, Phys. Rev. B **88**, 081102(R) (2013).
- [60] V. V. Karasiev, T. Sjostrom, J. W. Dufty, and S. B. Trickey, Phys. Rev. Lett. **112**, 076403 (2014).
- [61] S. Groth, T. Dornheim, T. Sjostrom, F.D. Malone, W. M. C. Foulkes, M. Bonitz, Phys. Rev. Lett. **119** (13) 135001 (2017). <http://dx.doi.org/10.1103/PhysRevLett.119.135001>.
- [62] Nathaniel R. Shaffer, Sanat Kumar Tiwari, and Scott D. Baalrud Pphysics of Plasmas **24**, 092703 (2017)
- [63] R. Bredow, T. Bornath, W.-D. Kraeft, and R. Redmer, Contrib. Plasma Phys. **53**, 276 (2013)
- [64] E. Liberatore, C. Pierleoni, and D. Ceperley, J. Chem. Phys. **134**, 184505 (2011).
- [65] J. Hammerberg and N. W. Ashcroft, Phys. Rev. B **9**, 409 (1974).
- [66] P. Jena and K. S. Singwi Phys. Rev. B, **17** 1592 (1978).
- [67] F. Perrot Phys. Rev. A **25**, 489 (1982).
- [68] Miguel A. Morales, Carlo Pierleoni, and D. M. Ceperley Phys. Rev. E **81** 021202 (2010).
- [69] F. Nardin, G. Jacucci and M.W.C. Dharma-wardana, Phys. Rev. A **37**, 1025-1028 (1988). [NRCC 28307]
- [70] L. Harbour, and G. D. Förster, M. W. C. Dharma-wardana, and L. J. Lewis, Physical review E **97**,043210 (2018). DOI: 10.1103/PhysRevE.97.043210 (2018).
- [71] F. Perrot, Y. Furutani and M.W.C. Dharma-wardana, Phys. Rev. A **41**, 1096-1104 (1990).
- [72] T. Kato, Commun. Pure Appl. Math. **10**, 151 (1957).
- [73] A. Theophilou, J. Chem. Phys. **149**, 074104 (2018).
- [74] A. Nagy, J. Chem. Phys. **149**, 204112 (2018).